19th Australasian Fluid Mechanics Conference
Melbourne, Australia
8-11 December 2014

LES Modelling of Mesocombustion Chambers with Arrhenius Complex Chemistry

P. Benard[1], V. Moureau[1], G. Lartigue[1] and Y. D'Angelo[1]

[1]CORIA - UMR6614 - Normandie Universite, Saint Etienne du Rouvray, France

Abstract

A quasi–cubic meso-scale 0.64 mm^3 hydrogen enriched air/methane whirl flow combustion chamber, with no moving parts, is analyzed by means of well-resolved LES. Unstructured 3D computations show that combustive flow structure, flame topology and global efficiency are quite in line with previous experimental and less detailed numerical modeling. Combustion is stabilized by a Central Recirculation Zone (CRZ) and mainly takes place in pre-mixed lean regime. Wall heat loss are also estimated and incomplete combustion zones are identified. The hydrogen-enriched case shows a quite significant effect on flame topology and combustion efficiency. Within the framework of thermo-electric applications, this (non-optimal) preliminary study is aimed at gathering and assessing modeling tools and efficient specific numerical strategies for shape and set–up optimization of the combustion chamber.

Introduction

In the past decade, much effort has been devoted to the investigation of combustion at the centimeter scale, or meso-scale combustion (see e.g. [5, 9]). As a portable source of heat or mechanical work, or as thermo–electric power generators, light small-sized devices would allow new applications using ~ 1 up to 100 W. Such systems would combine the benefits of being compact, durable, lightweight and instantly rechargeable. However, as the characteristic length of the object decreases, scaling issues may lead to unsustainable heat loss, more complex combustion regimes and/or incomplete combustion ([5]). Small scale can significantly affect flame stability, overall efficiency and pollutant formation. Meso-combustion hence deserves special attention. In the present paper, we shall focus on the 3D Large-Eddy Simulation of a quasi–cubic 0.64 mm^3 air/methane non-premixed asymmetric whirl flow [15, 4] combustion chamber, with no moving parts. In order for combustion to properly evolve and stabilize, mixing and residence time distribution should be enhanced, while keeping the hot gases and the flame far from the walls and controlling pollutant emissions.

The present study aims at gathering numerical tools & strategies for optimizing the combustion process inside the chamber, in the framework of thermo–electric applications.

Set-up

The investigated device is the meso-scale combustor studied experimentally in [8]. As shown in Fig. 1, the fluid volume is basically a cuboid which dimensions are $8 \times 8 \times 10\,\mathrm{mm}^3$. The chamber is fed by two inlets: one for fuel, with a 1 mm diameter, another for air, with a 0.8 mm diameter. The outlet diameter is 2 mm. The feeding system is complex as the air flow enters the combustor tangentially to the wall, while the fuel enters perpendicularly to the air jet. As previous experimental work [8] and simplified DNS modeling [12] showed, the air jet impinges at the upward wall, then deflects to create a very strong vortex at the center of the combustion chamber. The centrifugal forces drive lighter hot gases towards the center of the chamber (the Central Recirculation Zone or CRZ), while the colder gases are pushed towards the wall. This flow topology is expected to enhance mixing between air, fuel and combustion products and to improve flame stability.

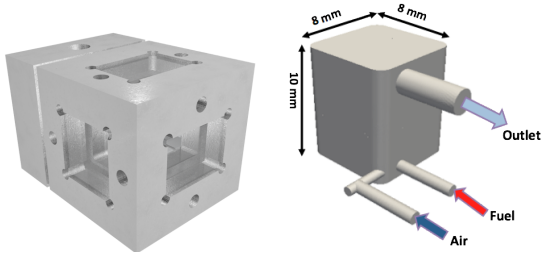

Figure 1: Three–dimensional modeling of the studied meso-combustor and schematic of the computed fluid volume.

Cases	C1	C2	C3
CH_4 mass flow rate $\dot{m}_{CH_4}$ $[\times 10^{-6}\mathrm{kg/s}]$	1.74	1.28	0.47
H_2 mass flow rate $\dot{m}_{H_2}$ $[\times 10^{-7}\mathrm{kg/s}]$	0.0	1.61	5.34
Air mass flow rate $\dot{m}_{air}$ $[\times 10^{-6}\mathrm{kg/s}]$	29.0	27.6	23.7
Equivalence ratio ϕ	1.03	1.00	1.12
Power injected P_{in} [W]	87.0	83.4	87.6
Wall temperature T_{wall} [K]	417	463	472

Table 1: Operating conditions for the considered computation.

The combustor was tested experimentally both with a pure CH_4/air mixture and H_2 enrichment. Here, we shall present and analyse only one pure CH_4/air and two H_2 enrichment cases, which operating conditions are summarized in Table 1. The Reynolds number based on the air inlet velocity and inlet diameter is around $Re = 2500$ so the flow is weakly turbulent. The reactants are injected at 300 K and pressure is 101325 Pa.

Numerical Modeling

Chemistry

The choice for chemistry modeling depends on the phenomena one wishes to evidence. Preliminary computations showed that tabulated chemistry approach (see e.g the FPI approach [6]) applied to this burner is not able to accurately capture transient combustion regimes[1], heat loss at the walls, or non-flamelet combustion. So a direct Arrhenius chemical kinetics approach was prefered, coupled with detailed transport. With this approach, since detailed modeling for kinetics can be prohibitively expensive, and reduced mechanisms may be thought of. However, making use of global or too simple kinetics (e.g. up to 2 or 4 steps), can lead to very poor pollutant predictions. As an example when using a two-step scheme, CO mass fraction can be underestimated by a factor larger than 3 [1]).

A suitable chemistry modeling for our case — both in terms of CPU cost and pollutant prediction accuracy, is Coffee's semi-

[1]e.g. mainly due to time and space varying temperature and composition inhomogeneities, as well as varying turbulent conditions.

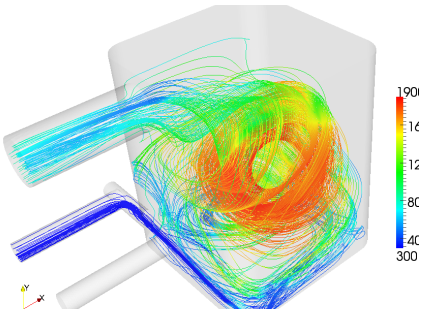

Figure 2: Streamlines of the flow inside the combustor colored by temperature.

detailed mechanism [2] that includes 14 species and 38 reactions.

However, even such semi-detailed chemistry requires expensive computation of complex reaction rates, and the involved system of ODE can be very stiff — that is indeed the case in the present study. The time step required for explicit resolution can be much smaller than the convective time step: down to 10^{-10} s to be compared with a typical convective time of 10^{-5} s for the low-Mach solver YALES2 [10, 11] used here.

The specialized library CVODE [3] dedicated to the time integration of stiff systems of ODE makes use of a variable order and variable time step Backward Differentiation Formula (BDF) with error control. To advance the system of PDE, a fractional-step procedure is used. Convection is first advanced in time with estimated diffusion and chemistry, then diffusion and chemistry are sub-stepped as in [13]. However, even with such a specific procedure, the CPU cost depends on the node location: the advancement of species equations is inexpensive in fresh and burnt gases, but much more expensive in the flame front, where reaction takes place. Thus, on one processor, the computational time depends on the number of nodes "belonging to the flame" it processes. Each processor needs to wait for the last one to achieve time stepping before going to the next time-step. To circumvent this issue, a dynamic load balancing strategy based on task stealing and the Message Passing Interface (MPI) library is adopted.

Results and Discussion

Flame Topology

The following results are shown using the pure CH_4 C1 case (Table 1).

The streamlines in Fig. 2 show how the reactants mix each other, creating the whirl flow recirculation, which becomes the Central Recirculation Zone (CRZ). As expected, the burnt gases are concentrated in the CRZ while fresh gases are confined close to the walls.

Figure 3 represents the flame front topology thanks to an instantaneous 3D view of an isocontour of the enthalpy source term. The flame is confined to the CRZ because of the quenching due to the walls. Small scale wrinkling is visible close to the fuel and air injections due to the jet dynamics while large scale wrinkling is present close to the outlet. Turbulence structures are illustrated in Fig. 4 by representing Q-criterion iso-contours. Small vortices created in the air jet wrinkle the flame front in the injection area. As the flow progresses into the combustor, less turbulent structures are present and the flame tends to adopt an almost laminar topology.

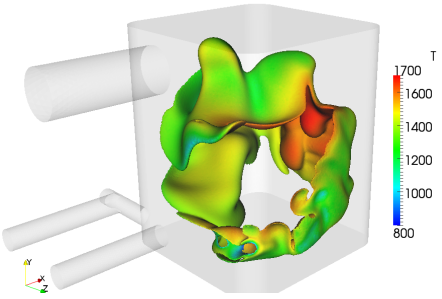

Figure 3: 3D view of the flame front position (defined as an iso-contour of ω_T) colored by temperature.

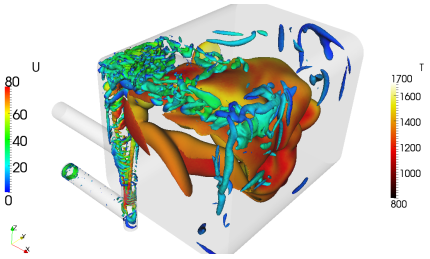

Figure 4: 3D view of the Q criterion colored by the velocity and the iso-contour of ω_T colored by the temperature.

Combustion Regime

In the burner, fuel and air are injected separately. Both premixed and non-premixed combustion may therefore occur. To gain more insight into the combustion regime, Takeno's index ξ [14] is analyzed. It is given by:

$$\xi = \frac{1}{2}\left(1 + \frac{\nabla Y_F \nabla Y_O}{|\nabla Y_F||\nabla Y_O|}\right). \quad (1)$$

$\xi = 1$ corresponds to premixed fronts while $\xi = 0$ indicates the presence of non-premixed fronts. Figure 5 shows that combustion takes place in the pre-mixed regime in most regions. Only a few zones close to the air and fuel injections exhibit non-premixed combustion.

Then, to quantify the degree of premixing, Fig. 6 shows the Probability Density Function (PDF) of the equivalence ratio φ for the control volumes belonging to the reaction zone. The maximum is located close to 0.9 and the shape of the PDF indicates that most of combustion takes place between $\varphi = 0.7$ and $\varphi = 1$, i.e. for lean conditions.

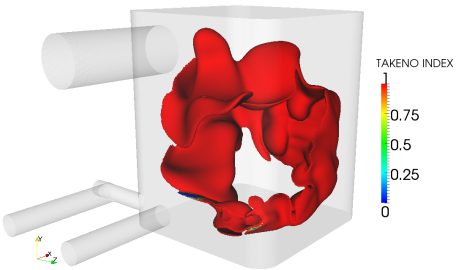

Figure 5: 3D view of the flame front position defined as an isocontour of ω_T colored by Takeno's index.

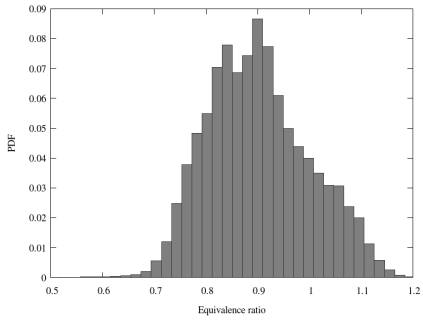

Figure 6: Probability Density Function of equivalence ratio φ, for reacting zones.

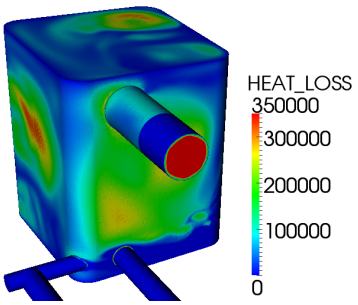

Figure 7: Instantaneous heat loss in W/m^2.

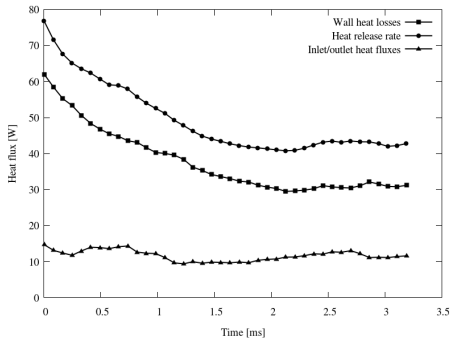

Figure 8: Time evolution of total (integrated) wall heat loss, heat release rate and inlet/outlet enthalpy fluxes in W.

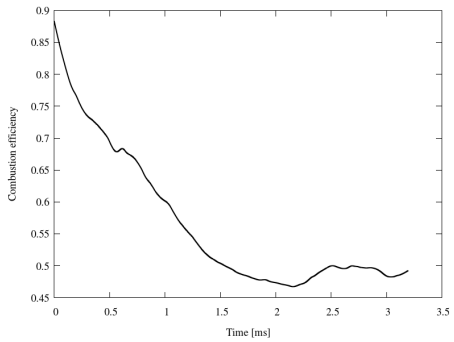

Figure 9: Time evolution of combustion efficiency P_r/P_{in}.

Burner Performances

To evaluate the burner performances, it is important to have a fait estimate of heat loss at the walls. The computation of heat loss at the walls, where a constant-temperature Dirichlet boundary condition is imposed, is not as straightforward as it may seem. It requires the calculation of the heat flux balance in control volumes at the wall. Imposing the Dirichlet boundary condition is indeed equivalent to imposing a variable heat flux at the wall, which keeps the temperature constant in the wall control volumes.

A snapshot of heat loss estimated by this technique is presented in Fig. 7. This figure shows that heat loss occur at the center of the cuboid faces due to the cooling effect of the injection jets. The level of heat loss is high and strongly affects combustion, pollutant emissions and burner efficiency.

In order to have an accurate evaluation of heat loss, the balance of enthalpy fluxes is plotted in Fig. 8 as a function of time t. The time $t = 0$ is taken as the time when the ignition forcing mimicking a spark plug is stopped. In this figure, the wall heat loss, the heat release rate and the sum of incoming and leaving enthalpy fluxes are represented. When convergence is reached, heat loss reaches 74% of heat release.

It may also be noted that the heat release rate P_r is quite lower than the expected power value P_{in} of 87 W. The ratio of both quantities is plotted in Fig. 9. It confirms that combustion is far from being complete.

Hydrogen Enrichment

In order to improve the global performances, hydrogen enrichment was also tested. Computations were performed using the C2 and C3 cases of Table 1, corresponding to 10% and 50% hydrogen mass enrichment respectively, and with the same chemical injected power as C1. Effects on flame topology and performances are observed. Figure 10 shows volumic rendering of the chemical energy source term which represents the flame. In the C2 case, the flame present the same topology than in C1 but seems to be more wrinkled. On the C3 case, the flame topology is different: it appears more confined and more close to the walls and air jet.

Performances and flame characteristics are summarized in the Table 2. The mean heat release increase with the hydrogen enrichment rate as the efficiency. It is a well-known effect of the hydrogen enrichment which combines three effects: larger laminar flame velocity, larger flame surface and turbulent stretch which affects the flame. So the conversion efficiency starts at 59% for the C1 case and is improved up to 70% thanks to hydrogen enrichment. The same trend has been observed experimentally.

The C2 more wrinkled flame allow to have an increasing of the flame surface of 25% which is expected [7]. As the flame topology is modified in the C3 case and appeared more confined, the flame surface is lower than for the C1 case. It could be explained thanks to the high laminar flame velocity of the C3 case, which permits the flame to be very close to the walls and to the air jet.

This analysis is encouraging in terms of fuel conversion but most of this additional power is lost at the walls. It can be explained by a too restrictive residence time and non-optimal combustion chamber geometry. However, hydrogen enrichment showed a positive effect on the pollutant emissions.

Since it promotes fuel conversion, hydrogen addition enhances combustion and released power. However, in the considered operating conditions, most of this additional power is lost at the

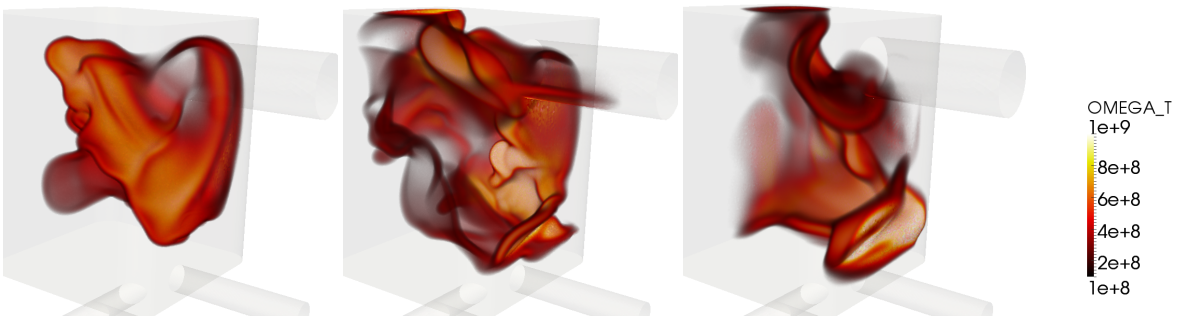

Figure 10: Volumic rendering of energy source term representing the flame on the C1, C2 and C3 cases.

Cases	C1	C2	C3
Mean heat release [W]	51.3	55.0	61.3
Efficiency [%]	59.0	65.9	70.0
Mean flame surface $[\times 10^{-4}\mathrm{m}^2]$	2.12	2.64	2.00
Heat rel. by flame surface unit $[\mathrm{kW/m}^2]$	247	208	307
Flame volume $[\times 10^{-8}\mathrm{m}^3]$	8.71	13.44	12.45
Flame charact. thichness $[\times 10^{-4}\mathrm{m}]$	4.1	5.1	6.2

Table 2: Combustion system performances and flame characteristics for the three cases.

walls. This can be explained by too restrictive a residence time and non-optimal combustion chamber geometry. However, hydrogen enrichment also allows for pollutant emissions decrease.

Conclusions

As already mentioned, within the framework of thermo-electric power generation, one of the main goals of the present work was to assess a computational tool for small-scale combustion chambers shape optimization, both in terms of energy efficiency and pollutant emissions. The combustion process in the small scale chamber must hence be as complete as possible and wall heat loss minimized. Such an optimization procedure may require to perform numerous computations of the complex chemistry combustive flow, while modifying the chamber shape and outlet/inlets position. We need sufficiently resolved simulations but at an affordable cost. More specifically, we found that for the pure methane case, the flow structure, flame-topology and combustion regimes computed are quite in line with previous experimental work [8] and less detailed numerical modeling [12]. In particular, the presence of the Central Recirculation Zone (or CRZ) is able to stabilize the flame in the centre of the chamber. Preliminary mixing of air and fuel is efficient enough for combustion to take place in the pre-mixed regime almost everywhere. The PDF of the equivalence ratio for reacting zones also shows that combustion mainly occurs in lean conditions. The resulting combustion efficiency (released energy/introduced energy) is about 50 %.

Hydrogen enrichment has a strong impact on the burner performances and affects the flame topology. However, the additional heat release is lost at the wall due to enhanced heat transfer. This shows there is still room for further optimization, both for more complete combustion and lesser wall loss.

Acknowledgements

This work was granted access to the HPC resources of CCRT and CRIHAN, under respectively the allocations x20132b6186 and 20080013.

References

[1] Albouze, G., Poinsot, T. & Gicquel, L., Chemical kinetics modeling and LES combustion model effects on a perfectly premixed burner, *C. R. Meca.*, **337**, 2009, 318-328.

[2] Coffee, T.P., Kinetic mechanisms for premixed, laminar, steady state methane/air flames. *Comb. Flame*, **55**, 1984, 161-170.

[3] Cohen, S. D. & Hindmarsh, A., CVODE, a Stiff/Nonstiff ODE Solver in C, *Comput. Phys.*, **10**, 1996, 138-143.

[4] Cozzi, F., Coghe, A. & Picheo, G., Experimental characterization of a meso-scale combustor by means of optical diagnostics, *XX AIDAA Congress*, 2009.

[5] Fernandez-Pello, A.C., Micropower generation using combustion: Issues and approaches, *Proc. Comb. Inst.*, **29**, 2002, 883-899.

[6] Gicquel, O., Darabiha, N. & Thevenin, D., Liminar premixed hydrogen/air counterflow flame simulations using flame prolongation of ILDM with differential diffusion, *Proc. Comb. Inst.*, **28**, 2000, 1901-1908.

[7] Hawkes, E. R. & Chen, J. H., Direct numerical simulation of hydrogen-enriched lean premixed methane–air flames, *Comb. Flame*, **138**, 2004, 242-258.

[8] Liu, S., Renou, B., Sjstrand, M., D'Angelo & Y., Cozzi, F., Experimental study of combustion and flow dynamics in a meso-scale whirl combustor, *15th Int. Symp. App. Laser Tech. Fluid Mech.*, 2010.

[9] Maruta, K., Micro and mesoscale combustion, *Proc. Comb. Inst.*, **33**, 2010, 125-150.

[10] Moureau, V., Domingo, P. & Vervisch, L., *C.R. Meca.*, **339**, 2011, 141-148.

[11] YALES2, *http://www.coria-cfd.fr*.

[12] Sjostrand, M., Ph.D. thesis, 2012.

[13] Yu, R., Yu, J. & Bai, X.-S., An improved high-order scheme for DNS of low Mach number turbulent reacting flows based on stiff chemistry solver, *Comp. Phys.*, **231**, 2012, 5504-5521.

[14] Yamashita, H., Shimada, M. & Takeno, T., A numerical study on flame stability at the transition point of jet diffusion flames, *Proc. Comb. Inst.*, **26**, 1996, 27-34.

[15] Yetter, R.A., Glassman, I. & Gabler, H.C., Asymmetric whirl combustion: A new low NOx approach, *Proc. Comb. Inst.*, **28**, 2000,1265-1272.